Justification

This manuscript is intended for the special edition to mark the 100th anniversary of the Fritz Haber Institute.

One of the major challenges in the development of clean energy fuel cells is the performance degradation of the electrocatalyst, which, apart from poisoning effects, can suffer from corrosion due to its exposure to a harsh environment under high potentials. In this communication, we demonstrate how interactions of Pt with a transition metal support affect not only, as commonly intended, the catalytic activity, but also the reactivity of Pt towards oxide formation or dissolution. We use two well-defined single-crystal model systems, Pt/Rh(111) and Pt/Au(111) and a unique x-ray spectroscopy technique with enhanced energy resolution to monitor the potential-dependent oxidation state of Pt, and find two markedly different oxidation mechanisms on the two different substrates. This information can be of great significance for future design of more active and more stable catalysts.

Abstract

We have studied the potential-induced degradation of Pt monolayer model electrocatalysts on Rh(111) and Au(111) single-crystal substrates. The anodic formation of Pt oxides was monitored using *in situ* high energy resolution fluorescence detection x-ray absorption spectroscopy (HERFD XAS). Although Pt was deposited on both substrates in a three-dimensional island growth mode, we observed remarkable differences during oxide formation that can only be understood in terms of strong Pt–substrate interactions throughout the Pt islands. Anodic polarization of Pt/Rh(111) up to +1.6 V vs. RHE (reversible hydrogen electrode) leads to formation an incompletely oxidized passive layer, whereas formation of PtO_2 and partial Pt dissolution is observed for Pt/Au(111).

SLAC National Accelerator Laboratory, Menlo Park, CA 94025

Work supported in part by US Department of Energy contract DE-AC02-76SF00515.

Fuel Cell Catalysis

DOI: 10.1002/anie.200((will be filled in by the editorial staff))

Degradation of Bimetallic Model Electrocatalysts – an *in situ* XAS Study

Daniel Friebel, Daniel J. Miller, Dennis Nordlund, Hirohito Ogasawara, Anders Nilsson**

Proton exchange membrane fuel cells (PEMFC) could be an important building block for a renewable energy infrastructure, converting chemically stored energy – e.g., from solar peak production – back into electricity for electric vehicles or stationary off-the-grid applications. An unaccomplished prerequisite for such a development is the availability of cost-efficient electrocatalyst materials, in particular for the oxygen reduction reaction (ORR). Pt-free catalysts made from earth-abundant materials[1][2] would be desirable, but exhibit too high overpotentials. Nevertheless, the cost of Pt-based catalysts can be reduced by tuning both the morphology and electronic structure to maximize activity. Significant enhancements can be achieved with bimetallic systems where the Pt 5*d*-band is shifted due to strain and ligand effects.[3-11] However, highly active carbon-supported Pt and Pt-alloy nanoparticles have been successfully tested only on short time scales, whereas degradation occurs under long-term operating conditions through sintering, Pt dissolution, carbon corrosion and nanoparticle-support detachment.[12][13] Furthermore, the enhanced catalytic activity of bimetallic nanoparticles is often achieved through a specific "core-shell" distribution of constituents,[3][14] which also lacks long-term stability.

Here, we present a study on the anodic oxidation of small Pt islands supported on single-crystal Rh(111) and Au(111) substrates, using *in situ* x-ray absorption spectroscopy (XAS) in the high energy resolution fluorescence detection (HERFD) mode. By depositing ultrathin Pt layers onto a M(111) substrate, we mimic the strain and vertical ligand effects that also occur in Pt alloys, but with better control of structure and element distribution and the highest possible surface sensitivity of the bulk-penetrating hard x-ray probe. Metallic Pt and different Pt oxides can be clearly identified by the shape and intensity of the characteristic maximum ("white-line") near the Pt L_3 absorption edge due to $2p \rightarrow 5d$ transitions.[15-17] The spectral resolution in conventional XAS is limited by the Pt 2*p* core hole lifetime broadening (~5.2 eV), but significantly sharpened spectral features can be obtained with the HERFD technique.[18][19]

The ORR activity for Pt overlayers on various transition metal substrates has been studied in detail with rotating disk electrode (RDE) measurements,[4] and a volcano plot using the adsorption strength of atomic oxygen as descriptor has been established using density functional theory (DFT).[5][20] While the ORR activities of the two systems studied here are of the same order of magnitude, they lie on opposite sides of the volcano, exhibiting weaker (Pt/Rh(111)) and stronger (Pt/Au(111)) O adsorption than pure Pt.

However, there is an apparent discrepancy between the theoretically predicted trend[5] and experimentally determined ORR activities for a number of Pt/M(111) systems prepared via redox displacement of underpotential-deposited Cu.[4][21] This disagreement can be explained if, instead of the uniform two-dimensional (2D) monolayers assumed in DFT calculations, redox displacement yields three-dimensional (3D) Pt islands. Indeed, 3D island growth has been confirmed with *in situ* scanning tunneling microscopy for electrochemically deposited Pt/Au(111).[22][23] On Rh(111), a 2D Pt layer can be grown by UHV evaporation onto a heated substrate,[24] and we recently studied electrochemical surface oxide formation on such a 2D Pt/Rh(111) sample with *in situ* HERFD XAS and EXAFS.[25] In contrast, the redox-displacement technique results in small 3D islands also for Pt/Rh(111); this is evident from *in situ* EXAFS (Supporting Information). We use this 3D Pt/Rh(111) sample in our comparison with Pt/Au(111) in order to provide a similar Pt morphology.

Interestingly, not only the *d*-band shifts and corresponding oxygen affinities for Pt/Au(111) and Pt/Rh(111), but also the surface energies of the substrate metals in these systems differ substantially. Au has a significantly lower surface energy than Pt,[26] which explains why Pt cannot be grown on Au in a layer-by-layer mode. Rh, in contrast, has a higher surface energy than Pt. We find that surface and cohesion energies strongly influence the redox chemistry of Pt islands at potentials above 1.0 V (RHE) where Pt oxides and hydrated Pt cations become thermodynamically stable. Such conditions can occur in various fuel cell operating scenarios[12] and contribute significantly to catalyst degradation.

In situ HERFD XAS measurements on Pt/Rh(111) (Fig. 1a) and Pt/Au(111) (Fig. 1b) show significant changes in the white-line region as the potential is increased above 1.0 V. On both samples we initially observe a transition from a narrow absorption maximum at 11566 eV to a much broader peak around 11567 eV; similar changes were observed in our previous study of 2D Pt/Rh(111).[25] However, while this new feature saturates on both 2D Pt/Rh(111) and 3D Pt/Rh(111) upon further increasing the potential, a second transition occurs on Pt/Au(111) after 1.4 V is reached. At this potential, a strong increase of the white-line intensity develops during a time-scale of ~40 min and the absorption maximum shifts to 11568 eV.

By comparison with *ab initio* multiple-scattering calculations using FEFF8.4[27] for various Pt oxides (Fig. 2), it is clear that the high white-line intensities observed for Pt/Au(111) above 1.4 V can only be explained with the formation of Pt(IV). The broader appearance and weaker peak intensity in the measurement can be attributed to either additional Pt in lower oxidation states, or to a disordered PtO_2 structure.

[*] Dr. D. Friebel, D. J. Miller, Dr. Dennis Nordlund, Dr. H. Ogasawara, Prof. A. Nilsson
SLAC National Accelerator Laboratory
2575 Sand Hill Rd, Menlo Park, CA 94025, USA
Fax: (+1) 650 926 4100
E-mail: dfriebel@slac.stanford.edu, nilsson@slac.stanford.edu

[**] This work is supported by the Department of Energy, Office of Basic Energy Sciences, Division of Materials Sciences and Engineering, under contract DE-AC02-76SF00515. This research was partly carried out at the Stanford Synchrotron Radiation Lightsource, a National User Facility operated by Stanford University on behalf of the U.S. Department of Energy, Office of Basic Energy Sciences.

Supporting information for this article is available on the WWW under http://www.angewandte.org or from the author.

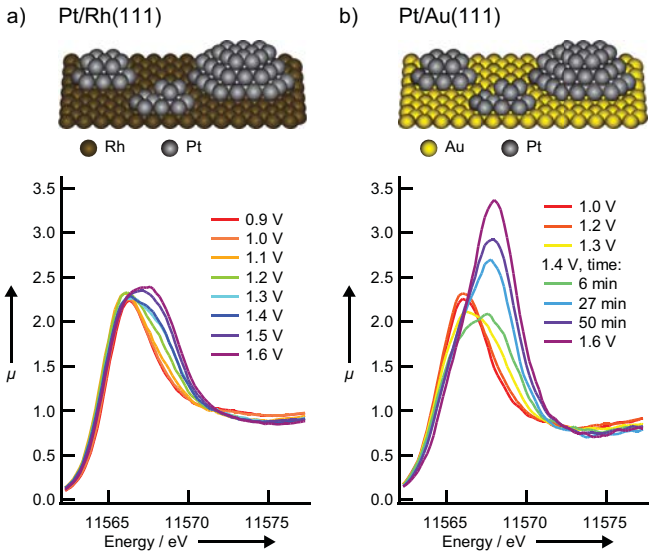

Figure 1. *In situ* Pt L_3 HERFD XAS for a) Pt/Rh(111), b) Pt/Au(111) in 0.01 M $HClO_4$. Spectra were recorded in the order of increasing electrochemical potential. For Pt/Au(111) we also show a time-series single XAS sweeps at 1.4 V.

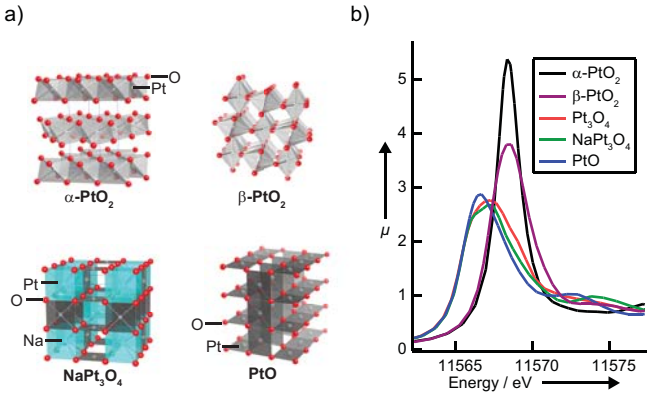

Figure 2. a) Structure models and b) calculated HERFD XAS spectra of different Pt oxides using FEFF8.4.

The potential dependence of the amount of oxide formation can be followed using integrated white-line intensities as shown in Fig. 3a. Oxide formation on Pt/Rh(111) appears sluggish throughout the potential range studied. Similar behavior was found with XAS on 2D Pt/Rh(111),[25][28] and with *in situ* x-ray diffraction on Pt(111),[28] and a Pt–O place-exchange mechanism was proposed.[28][29] In contrast, a sharp increase of the average Pt oxidation state can be seen for Pt/Au(111) at 1.4 V, pointing towards a significantly faster phase transition at this potential. Moreover, oxide formation on Pt/Au(111) coincides with Pt dissolution (Fig. 3b), whereas dissolution from Pt/Rh(111) is not detectable within uncertainties arising from sample/beam alignment. We conjecture that the rapid oxide growth at 1.4 V is facilitated by an alternative oxidation pathway where Pt is dissolved as Pt^{2+}, followed by further oxidation of Pt^{2+} to Pt^{4+} which precipitates as oxide, thus avoiding sluggish Pt–O solid-state diffusion.

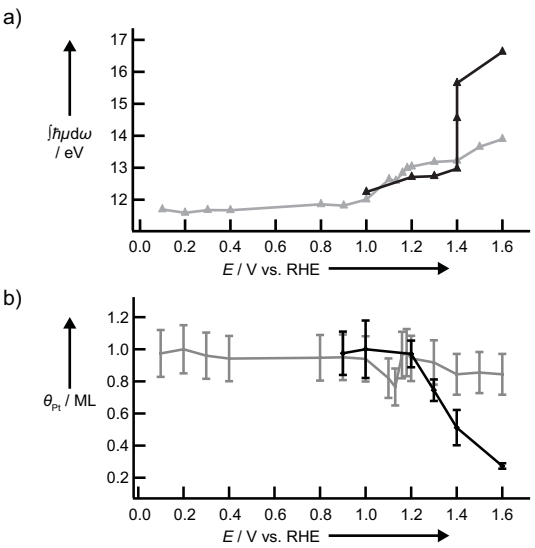

Figure 3. a) Potential dependence of Pt oxide formation for Pt/Rh(111) and Pt/Au(111); the increase of the integrated white line intensity indicates the extent of Pt oxidation. b) Pt coverage, determined from relative fluorescence count rates at 11600 eV incident energy, as function of increasing potentials; note the anodic dissolution of Pt/Au(111).

The unusually strong tendency of Pt/Au(111) towards Pt dissolution can be explained with a general destabilization of Pt islands on Au surfaces due to the surface energy mismatch. Surface Pt tends to be removed in favour of exposing Au which has much lower surface energy, either, at high potentials, by anodic dissolution,[30][31] or by diffusion into the Au substrate.[31-33] Pt oxide formation should follow a similar thermodynamic dependence on Pt island stability as dissolution; this, however, may be obscured by the complex kinetics of the Pt–O place exchange. In analogy to a trend shown for 4*d* transition metals,[34] increased Pt cohesion in Pt/Au(111) due to the *d*-band shift may destabilize subsurface oxygen, a precursor to oxide formation.

In summary, our XAS results clearly show that anodic Pt dissolution is promoted on an Au(111) substrate, whereas anodic polarization of Pt/Rh(111) leads instead to passivation. We can expect Pt/Rh(111) or Pt/Rh nanoparticles to provide good long-term stability under ORR conditions. However, the catalytic activity is suboptimal, and several other substrates with high surface energy, e.g., Ir and Ru, also shift the Pt 5*d* band too far toward the weak Pt–O interaction side of the fuel cell volcano plot. Therefore, it may be necessary to find a compromise in ORR catalyst design between high activity and long-term stability.

Received: ((will be filled in by the editorial staff))
Published online on ((will be filled in by the editorial staff))

Keywords: x-ray spectroscopy · catalysis · electrochemistry · fuel cells · ab initio calculations

[1] B. B. Blizanac, P. N. Ross, N. M. Markovic, *Electrochim. Acta* **2007**, *52*, 2264–2271.
[2] R. Bashyam, P. Zelenay, *Nature* **2006**, *443*, 63–66.
[3] P. Strasser, S. Koh, T. Anniyev, J. Greeley, K. More, C. Yu, Z. Liu, S. Kaya, D. Nordlund, H. Ogasawara, et al., *Nature Chem.* **2010**, *2*, 454–460.
[4] J. L. Zhang, M. B. Vukmirovic, Y. Xu, M. Mavrikakis, R. R. Adzic,

Angew. Chem., Int. Ed. **2005**, *44*, 2132–2135.
[5] J. Greeley, I. E. L. Stephens, A. S. Bondarenko, T. P. Johansson, H. A. Hansen, T. F. Jaramillo, J. Rossmeisl, I. Chorkendorff, J. K. Nørskov, *Nature Chem.* **2009**, *1*, 552–556.
[6] K. Sasaki, Y. Mo, J. X. Wang, M. Balasubramanian, F. Uribe, J. McBreen, R. R. Adzic, *Electrochim. Acta* **2003**, *48*, 3841–3849.
[7] J. Zhang, K. Sasaki, E. Sutter, R. R. Adzic, *Science* **2007**, *315*, 220–222.
[8] R. Zeis, A. Mathur, G. Fritz, J. Lee, J. Erlebacher, *J. Power Sources* **2007**, *165*, 65–72.
[9] V. R. Stamenkovic, B. Fowler, B. S. Mun, G. F. Wang, P. N. Ross, C. A. Lucas, N. M. Markovic, *Science* **2007**, *315*, 493–497.
[10] V. R. Stamenkovic, B. S. Mun, M. Arenz, K. J. J. Mayrhofer, C. A. Lucas, G. F. Wang, P. N. Ross, N. M. Markovic, *Nat. Mater.* **2007**, *6*, 241–247.
[11] H. Wolfschmidt, R. Bussar, U. Stimming, *J. Phys.: Condens. Matter* **2008**, *20*, 374127.
[12] R. Borup, J. Meyers, B. Pivovar, Y. S. Kim, R. Mukundan, N. Garland, D. Myers, M. Wilson, F. Garzon, D. Wood, et al., *Chem. Rev.* **2007**, *107*, 3904–3951.
[13] S. S. Zhang, X. Z. Yuan, J. N. C. Hin, H. J. Wang, K. A. Friedrich, M. Schulze, *J. Power Sources* **2009**, *194*, 588–600.
[14] J. Zhang, F. H. B. Lima, M. H. Shao, K. Sasaki, J. X. Wang, J. Hanson, R. R. Adzic, *J. Phys. Chem. B* **2005**, *109*, 22701–22704.
[15] J. A. Horsley, *J. Chem. Phys.* **1982**, *76*, 1451–1458.
[16] A. N. Mansour, J. W. Cook, D. E. Sayers, *J. Phys. Chem.* **1984**, *88*, 2330–2334.
[17] A. N. Mansour, D. E. Sayers, J. W. Cook, D. R. Short, R. D. Shannon, J. R. Katzer, *J. Phys. Chem.* **1984**, *88*, 1778–1781.
[18] F. M. F. de Groot, M. H. Krisch, J. Vogel, *Phys. Rev. B* **2002**, *66*, 195112.
[19] O. V. Safonova, M. Tromp, J. A. van Bokhoven, F. M. F. de Groot, J. Evans, P. Glatzel, *J. Phys. Chem. B* **2006**, *110*, 16162–16164.
[20] J. K. Nørskov, J. Rossmeisl, A. Logadottir, L. Lindqvist, J. R. Kitchin, T. Bligaard, H. Jonsson, *J. Phys. Chem. B* **2004**, *108*, 17886–17892.
[21] S. R. Brankovic, J. X. Wang, R. R. Adzic, *Surf. Sci.* **2001**, *474*, L173–L179.
[22] H. F. Waibel, M. Kleinert, L. A. Kibler, D. M. Kolb, *Electrochim. Acta* **2002**, *47*, 1461–1467.
[23] S. Strbac, S. Petrovic, R. Vasilic, J. Kovac, A. Zalar, Z. Rakocevic, *Electrochim. Acta* **2007**, *53*, 998–1005.
[24] M. Duisberg, M. Dräger, K. Wandelt, E. L. D. Gruber, M. Schmid, P. Varga, *Surf. Sci.* **1999**, *433*, 554-558.
[25] D. Friebel, D. J. Miller, C. P. O`Grady, T. Anniyev, J. Bargar, U. Bergmann, H. Ogasawara, K. T. Wikfeldt, L. G. M. Pettersson, A. Nilsson, *Phys. Chem. Chem. Phys.* **2011**, *13*, 262–266.
[26] E. Bauer, J. H. van der Merwe, *Phys. Rev. B* **1986**, *33*, 3657–3671.
[27] A. L. Ankudinov, B. Ravel, J. J. Rehr, S. D. Conradson, *Phys. Rev. B* **1998**, *58*, 7565–7576.
[28] H. You, D. J. Zurawski, Z. Nagy, R. M. Yonco, *J. Chem. Phys.* **1994**, *100*, 4699–4702.
[29] G. Jerkiewicz, G. Vatankhah, J. Lessard, M. P. Soriaga, Y. S. Park, *Electrochimica Acta* **2004**, *49*, 1451–1459.
[30] J. Greeley, J. Nørskov, *Electrochimica Acta* **2007**, *52*, 5829-5836.
[31] B. L. Abrams, P. C. K. Vesborg, J. L. Bonde, T. F. Jaramillo, I. Chorkendorff, *J. Electrochem. Soc.* **2009**, *156*, B273–B282.
[32] Y. Gohda, A. Gross, *J. Electroanal. Chem.* **2007**, *607*, 47–53.
[33] M. Ø. Pedersen, S. Helveg, A. Ruban, I. Stensgaard, E. Lægsgaard, J. K. Nørskov, F. Besenbacher, *Surface Science* **1999**, *426*, 395-409.
[34] M. Todorova, W. X. Li, M. V. Ganduglia-Pirovano, C. Stampfl, K. Reuter, M. Scheffler, *Phys. Rev. Lett.* **2002**, *89*, 096103.

Entry for the Table of Contents (Please choose one layout)

Layout 1:

Fuel Cell Catalysis

Daniel Friebel*, Daniel J. Miller, Dennis Nordlund, Hirohito Ogasawara, Anders Nilsson* _____ **Page – Page**

Degradation of Bimetallic Model Electrocatalysts – an *in situ* XAS Study

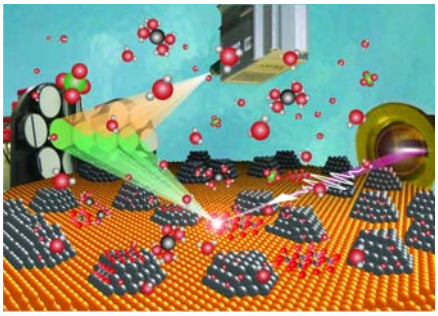

Gold destabilizes platinum surface atoms. Driven by the low surface energy of Au, Pt is removed from the surface. Depending on the electrochemical potential this can occur through Pt dissolution – either into the Au substrate, or, as demonstrated here, into the electrolyte. *In situ* HERFD XAS measurements indicate formation of PtO_2 via a dissolution-precipitation mechanism.

Supporting Information

Methods

Sample preparation. For the redox displacement of a Cu monolayer, Rh(111) (8 mm diameter, Surface Preparation Laboratory, Zaandam, The Netherlands) and Au(111) (4 mm diameter, MaTeck GmbH, Jülich, Germany) single crystals were prepared by flame annealing and subsequent cooling in a H_2/N_2 (5:95) atmosphere. The crystals were then transferred into a nitrogen-filled glovebag and mounted in a hanging meniscus flow cell which allows for a rapid exchange of the electrolyte under potential control. A Cu deposition voltammogram in 1 mM $CuSO_4$ + 0.05 M H_2SO_4 solution was then recorded at a cathodic potential sweep rate of 10 mV/s starting from +400 mV (Ag/AgCl). Immediately after the completion of the Cu upd peak, the cell was flushed with the Cu-free supporting electrolyte (0.05 M H_2SO_4). Meanwhile, the cathodic potential sweep was continued to a final value of -400 mV in order to prevent any dissolution of the Cu monolayer. In analogy to previous experiments [1,2] which used the stabilization of a Cu upd layer on Au(111) in Cu-free electrolyte, we are able to verify with cyclic voltammetry that the Cu layer remains stable and has the desired coverage of 1 ML. After the deposition of 1 ML Cu and its stabilization in Cu-free supporting electrolyte, the M(111) samples were quickly transferred to a glass beaker where the polished surface was exposed to the Pt deposition solution (1 mM K_2PtCl_4 + 0.05 M H_2SO_4) for ca. 30 s.

***In situ* x-ray electrochemical cell.** Two different *in situ* x-ray electrochemical cells were used in this study. A "thin layer" cell similar to earlier *in situ* x-ray diffraction setups [3] was used with 6 μm mylar foil (Goodfellow) as x-ray window. For every change of the potential the cell was inflated and, at the new potential value, kept under thick-layer conditions for at least 15 min in order to allow for potential-induced phase transitions to complete, before returning to the thin-layer mode for the next XAS measurement. Faster potential changes and higher electrochemical currents can be achieved in our "droplet" hanging meniscus cell [4], where a thick electrolyte layer is provided throughout the x-ray measurement. Both cells provide a three-electrode configuration with Pt wire as the counter electrode and a leak-free Ag/AgCl reference electrode. All electrode potentials were converted to the scale of the reversible hydrogen electrode (RHE).

All electrolytes were made from high-purity chemicals (70% $HClO_4$, Trace Select Ultra, Sigma-Aldrich and 95% H_2SO_4, Trace Select, Sigma-Aldrich; 99.999% $CuSO_4 \cdot 5\ H_2O$, Sigma-Aldrich) and ultrapure water from a Millipore Gradient system.

X-ray absorption spectroscopy. HERFD-XANES measurements were performed at SSRL Beam Line 6-2 using a Si(111) monochromator in combination with a Rowland circle analyzer spectrometer [5] consisting of three spherically bent Ge perfect crystals (R = 1 m). The crystals were aligned in a backscattering geometry using the (660) Bragg reflection at 80.0° to select the Pt $L\alpha_1$ fluorescence line (9442 eV). The combined resolution of the monochromator and analyzer as determined by measuring the elastic scattering was 1.4 eV. Assuming an intrinsic monochromator resolution of ~1 eV, the analyzer resolution is estimated to be ~1 eV.

The incidence angle of the x-ray beam to the Pt/M(111) surfaces was adjusted to the critical angle for total external reflection, thereby enhancing the fluorescence intensity up to fourfold [6]. The orientation of the electric field vector of the incident beam was perpendicular to the surface normal.

Computational methods. FEFF 8.4 calculations of HERFD XAS spectra were performed using the same parameters as described in detail in a previous study [4].

EXAFS characterization of 3D Pt/Rh(111)

During the deposition of Pt on Rh(111), one would expect, due to the high surface energy of Rh and attractive Pt–Rh interactions [7], that a growth mode of either the Frank-van der Merwe or Stranski-Krastanov type would be favored, i.e. at least up to a coverage of one monolayer, Pt would uniformly grow in a single 2D layer. Such a 2D Pt layer can actually be prepared under UHV conditions on Rh(111) [4,8]. However, significantly different results were obtained both with EXAFS when we prepared Pt/Rh(111) using the redox displacement of upd Cu. In Table S1, the latter sample shows a higher coordination number of Pt with nearest-neighbor Pt atoms and, more importantly, a significantly reduced Rh coordination, the latter indicating that a significant portion of the Pt atoms is not residing within the first layer above the topmost Rh(111) plane. Since at the same time the Pt–Pt coordination number is still significantly lower than the value of 12 for bulk Pt, we propose that the deposit consists of small three-dimensional islands. We conjecture that, under the growth conditions under electrolyte at room temperature, high kinetic barriers allow neither surface diffusion nor a dissolution-redeposition mechanism for a rearrangement towards the more stable two-dimensional morphology within the timescale of our experiment. For Pt/Au(111), we also assume a similar 3D morphology of the Pt deposit. This is favorable due to the much lower surface energy of Au compared to Pt [7]. Furthermore, three-dimensional growth has been demonstrated for the direct electrochemical deposition of Pt on Au(111) [9], and with HERFD XAS we find no significant difference in the potential-dependent behavior of Pt/Au(111) samples prepared either by direct electrodeposition or by the redox-displacement technique.

Table S1. ***In Situ*** **EXAFS Fitting Results for 1 ML Pt/Rh(111) Samples Prepared in UHV and by Redox-Displacement**

	Pt/Rh(111), evaporated, E = 0.0 V	Pt/Rh(111), redox-displacement, E = 0.1 V
$N_{Pt–Pt}$	6.5 ± 0.8	7.3 ± 0.7
$d_{Pt–Pt}$ (Å)	2.72 ± 0.02	2.74 ± 0.02
σ^2 (Å^2)	0.005	0.005
$N_{Pt–Rh}$	3.2 ± 0.7	1.4 ± 0.5
$d_{Pt–Rh}$ (Å)	2.72 ± 0.02	2.68 ± 0.05
σ^2 (Å^2)	0.005	0.005
R factor	0.0282	0.0238

References

[1] D. Friebel, C. Schlaup, P. Broekmann, K. Wandelt, *Surf. Sci.* **2006**, *600*, 2800–2809.
[2] D. Friebel, C. Schlaup, P. Broekmann, K. Wandelt, *Phys. Chem. Chem. Phys.* **2007**, *9*, 2142–2145.
[3] B. M. Ocko, J. Wang, A. Davenport, H. Isaacs, *Phys. Rev. Lett.* **1990**, *65*, 1466–1469.
[4] D. Friebel, D. J. Miller, C. P. O'Grady, T. Anniyev, J. Bargar, U. Bergmann, H. Ogasawara, K. T. Wikfeldt, P. L. G. M., A. Nilsson, *Phys. Chem. Chem. Phys.* **2011**, *13*, 262–266.
[5] P. Glatzel, U. Bergmann, *Coord. Chem. Rev.* **2005**, *249*, 65–95.
[6] G. A. Waychunas, in *Reviews in Mineralogy & Geochemistry*, Vol. 49, Mineralogical Soc America, **2002**, pp. 267–315.
[7] E. Bauer, J. H. van der Merwe, *Phys. Rev. B* **1986**, *33*, 3657–3671.
[8] M. Duisberg, M. Dräger, K. Wandelt, E. L. D. Gruber, M. Schmid, P. Varga, *Surf. Sci.* **1999**, *433*, 554–558.
[9] H. F. Waibel, M. Kleinert, L. A. Kibler, D. M. Kolb, *Electrochim. Acta* **2002**, *47*, 1461–1467.